



LAWRENCE  
LIVERMORE  
NATIONAL  
LABORATORY

UCRL-CONF-155626

# **Phosphate laser glass for NIF: production status, slab selection and recent technical advances**

*T. I. Suratwala, J. H. Campbell, P. E. Miller,  
C. B. Thorsness, M.O. Riley, P. R. Ehrmann,  
and R. A. Steele*

**December 30, 2003**

2004 SPIE  
Photonics West  
San Jose, CA  
January 27-29, 2004

This document was prepared as an account of work sponsored by an agency of the United States Government. Neither the United States Government nor the University of California nor any of their employees, makes any warranty, express or implied, or assumes any legal liability or responsibility for the accuracy, completeness, or usefulness of any information, apparatus, product, or process disclosed, or represents that its use would not infringe privately owned rights. Reference herein to any specific commercial product, process, or service by trade name, trademark, manufacturer, or otherwise, does not necessarily constitute or imply its endorsement, recommendation, or favoring by the United States Government or the University of California. The views and opinions of authors expressed herein do not necessarily state or reflect those of the United States Government or the University of California, and shall not be used for advertising or product endorsement purposes.

# Phosphate laser glass for NIF: production status, slab selection and recent technical advances

T. I. Suratwala<sup>\*</sup>, J. H. Campbell, P. E. Miller, C. B. Thorsness,  
M. O. Riley, P. R. Ehrmann, and R. A. Steele

Lawrence Livermore National Laboratory, P.O. Box 808 L-491, Livermore, CA 94551

## ABSTRACT

The National Ignition Facility (NIF) at the Lawrence Livermore National Laboratory is a stadium-sized high-energy (1.8 megajoule) / high-peak power (500 terawatt) laser system, which will utilize over 3000 meter-size Nd-doped metaphosphate glasses as its gain media. The current production status, the selection criteria of individual slabs for specific beam line locations, and some recent technical advances are reviewed. The glass blanks are manufactured by a novel continuous glass melting process, and the finished slabs are then prepared by epoxy bonding a Cu-doped phosphate glass edge cladding and by advanced finishing techniques. To date, nearly 3400 slab equivalents have been melted, 2600 have been rough-cut to blanks, 1200 have been finished, and 144 have been installed in NIF. A set of selection rules, which are designed to optimize laser performance (e.g., maintain gain balance between beam lines and minimize beam walkoff) and to maximize glass lifetime with respect to Pt damage site growth, have been established for assigning individual slabs to specific beam line locations. Recent technical advances for amplifier slab production, which include: 1) minimizing surface pitting (hazing) after final finishing; 2) minimizing humidity-induced surface degradation (weathering) upon storage and use; and 3) preventing mounting-induced surface fractures upon installation, have contributed in improving the laser glass quality.

**Keywords:** phosphate laser glass, high peak-power laser, National Ignition Facility, surface pitting, weathering, indentation fracture

## 1. INTRODUCTION

The National Ignition Facility (NIF), a high-peak power laser used for the study of high energy density plasma physics and fusion energy ignition, is currently being installed with optics for full-scale operation in 2008. NIF is comprised of 192 independent large aperture (40 x 40 cm<sup>2</sup>) laser beams capable of delivering 1.8 MJ of energy in a 3.5 ns pulse [1-2]. The heart of the laser is the meter-size Nd-doped phosphate laser glass. The NIF is capable of holding up to 18 amplifier slabs per beam line which would require 3400-3600 amplifier slabs, including spares. Similarly, another high power laser, Laser MegaJoule [3] currently under construction in France will require nearly 4500 glass slabs. The combined glass of the two laser systems require ~8000 slabs or 125 m<sup>3</sup> or 330 metric tons of finished optical quality glass. The amplifier glass is made from two commercially available Nd-doped meta-phosphate glasses (LG-770 glass from Schott Glass Technologies and LHG-8 from Hoya Corporation, USA), both of which were prepared by a continuous melting process.

Previous reviews on NIF laser glass have focused on laser glass composition and properties and the technical advances for making continuously melted glass in large volumes and with high optical quality [4-8]. The following review serves as an update to the previous reviews. We first briefly describe the continuous melting process and finishing method for fabrication of the amplifier slabs, and then provide the current NIF slab production status (Section 2). Then in Section 3 we describe some of the criteria being considered in selecting individual amplifier slabs for specific slab locations in the NIF beam lines. Finally, in Section 4, we describe some of the recent technical advances in successfully using the amplifier slabs. These include: 1) minimizing surface pitting (hazing) after final finishing (Sec. 4.1); 2) minimizing humidity-induced surface degradation (weathering) upon storage and use (Sec. 4.2); and 3) preventing mounting-induced surface fractures upon installation in NIF (Sec. 4.3). The mechanism for each of these phenomena and their mitigation are described.

---

<sup>\*</sup> suratwala1@llnl.gov; phone 1 925 422 1884; fax 1 925 423 0792; www.llnl.gov

## 2. AMPLIFIER SLAB FABRICATION AND PRODUCTION STATUS

### 2.1 Continuous Melting and Finishing

The continuous laser glass melting process, shown schematically in Fig. 1, converts high-purity, powdered raw materials into one continuously moving strip of high optical-quality laser glass. The laser glass melting process requires seven different operations carried out in separate vessels; to make the process continuous, the vessels are interconnected [5]. The first process unit is designed to mix and dry the high purity raw materials with minimal contamination. The laser glass specifications require that the raw materials contain only trace amounts ( $\leq 10$  ppm) of most common transition metal ions and less than 0.1 wt% of either physically or chemically absorbed water. The second unit is the melter system, which dissolves the powdered raw materials into a pool of molten glass and mixes these ingredients using convection currents inside the melter. The melter consists of custom designed high-purity refractory materials and employs a proprietary electrical heating system.

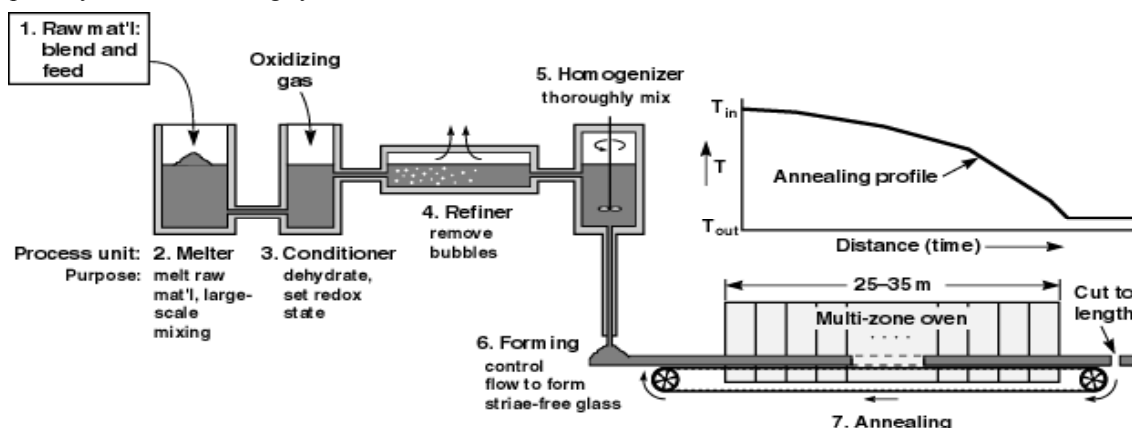


Fig. 1. Schematic representation of the continuous laser glass melting systems being used to manufacture laser glass.

All units beyond the melter are lined with high-purity platinum metal, as are the interconnecting pipes. Platinum is required to achieve the part-per-million optical homogeneity necessary for laser applications. However, the platinum can contaminate the glass with microscopic metallic inclusions. When a high-power laser beam hits an inclusion it causes it to explode, generating small fractures within the glass. To overcome this, we developed a unique conditioner unit (the third unit in the process) that uses oxygen and chlorine to greatly reduce platinum inclusions as well as any residual water. This is perhaps the most complex unit in the whole system.

The glass from the conditioner next moves to a refiner section where bubbles are removed using a combination of proprietary additives and high temperature. From here the glass enters the homogenizing unit and is thoroughly mixed to achieve the one-part-per-million chemical uniformity required to meet optical homogeneity specifications. The glass then flows through a platinum tube to a mold where it is formed into one continuously moving strip 5 to 8-cm thick, and about 0.5-m wide. The glass strip then passes through a custom-designed annealing oven where it is gradually cooled from more than 600°C to room temperature. Plates of laser glass ( $\sim 1 \text{ m} \times 0.5 \text{ m}$  for our specific application) are then cut from the end of this strip as it exits the production system.

Laser glass was previously manufactured by a discontinuous, one-at-a-time melting process. The discontinuous melting process involves first melting raw materials in a refractory vessel, then manually transferring to a second platinum-lined vessel, and then finally manually casting the glass into a mold [5]. The whole process must then be repeated to make the next glass piece. This process has a small throughput of two to three pieces per week. In addition, product quality can vary from one melt to the next simply because of small run-to-run variations in processing conditions. Most importantly, the product cost is high ( $> \$5000/\text{liter}$ ). Continuous glass melting, on the other hand, not only has the advantage of a much greater production rate of 70 to 300 pieces per week, but also little, if any, measurable variation in glass properties from one glass plate to the next. Also, the cost is dramatically lower ( $\leq \$1000/\text{liter}$ ).

The as-formed glass is then fabricated into glass blanks, which are rough-cut, inspection-polished slabs. Then the blanks are shipped to the finishing vendor (Zygo Corporation) to perform the epoxy bonding of the edge cladding [6] and final

finishing to be then termed a finished slab. The final finishing process involves deterministic grinding and advanced lap-polishing techniques developed by Zygo Corporation [9]. Photos of a finished amplifier slab are shown in Fig. 2.



**Fig. 2.** (Left) Photo of a finished amplifier slab; (Right) Photo of an amplifier slab LRU being assembled at LLNL.

### 2.3 Production Status and Glass Quality

To date, 100% of the amplifier glass to be installed on NIF has been melted as well as a significant number of “spare” slabs that are held in reserve for use over NIF’s expected 30-year life. Fig. 3 shows the current production status of amplifier glass at the Blank and Finished stage and the predicted rate of production in the outgoing years. Also shown is the demand curve representing the number of finished slabs installed in NIF. The demand curve represents the rate at which amplifier slabs are installed on NIF assuming an 11-5 configuration (11 amplifiers in the Main Amplifier and 5 in the Power Amplifier). To date, ~2600 blanks have been prepared and ~1200 finished slabs are ready for installation in NIF. 144 amplifier slabs have been installed in NIF.

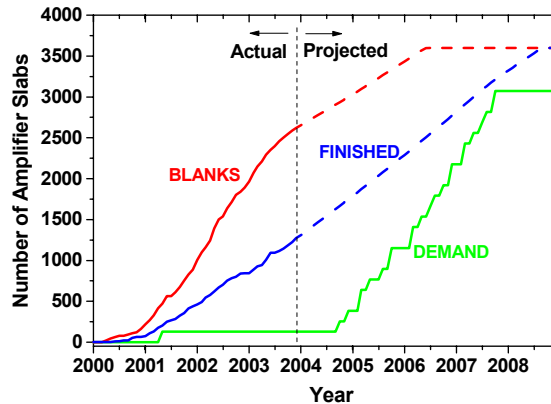


**Fig. 3.** Production status and predicted amplifier blank and finished production rate for NIF.

The finished slabs have properties that are typically well within specification. Table 1 lists quality assurance (QA) measurements performed on almost each Hoya (LHG-8) and Schott (LG-770) slab as well as the corresponding design specification. The value in parenthesis represents plus or minus one standard deviation on the slabs measured to date. The absorptivity at 400 nm can be correlated to the amount of dissolved Pt in the glass; the absorptivity at 1053 nm (the operating laser wavelength) is a measure or check of dissolved absorbing impurities (e.g.  $\text{Cu}^{2+}$ ,  $\text{Fe}^{3+}$ , and other transition metals) in the glass. The absorptivity at 3333 nm is a measure of the hydroxyl group content (OH) in the glass; OH groups reduce the Nd fluorescence lifetime through non-radiative losses thus reducing the energy stored in the slab [13]. Details of the various factors affecting the laser glass performance as well as a detailed list of thermal, mechanical, optical and laser properties of the glass can be found elsewhere [4,5,8,13,17]. Note that the transmitted wave front quality of the finished slabs is significantly better than the NIF specifications. For example, the Peak-to-Valley transmitted wavefront over the whole optic surface approaches on average  $\lambda/5$  where as the specification is  $\lambda/3$ .

In addition to the QA measurements listed in Table 1, each laser slab is also raster-scanned with the output from a commercial Nd-YAG Q-switched laser (1053 nm, 6 J/cm<sup>2</sup>, 8 ns) to initiate damage at any Pt inclusions that may be present. Pt inclusions in the glass will absorb the high fluence light in the laser and explode to create localized fractured damage sites. Because these tiny inclusions (1-10  $\mu$ m) are difficult to detect in the “un-scanned” slabs, the slabs are raster scanned to initiate damage and “grow” it to the point it can be easily detected by visual inspection. During the post-scan inspection process, the size and location of all the Pt-sites are recorded. Each slab is then graded based on the number and size of these sites and assigned a “Tab-number” grade using the convention shown in Table 2. Also shown, is the percentage of each Tab grade for NIF Blanks processed to date. Note that of the 27% “Tab-1” slabs more than 70% have no Pt inclusions.

**Table 1:** Values of some of the measured properties of amplifier slabs during glass melting and finishing compared with specification.

Property	LG-770	LHG-8	NIF Specification
	Average (St. Dev)	Average (St. Dev)	
Nd Doping (10 <sup>20</sup> ion/cm <sup>3</sup> )	4.19 ( $\pm$ 4%)	4.23 ( $\pm$ 1%)	4.22 $\pm$ 0.1
Absorption at 400 nm (cm <sup>-1</sup> )	0.224 ( $\pm$ 10%)	0.079( $\pm$ 10%)	$\leq$ 0.25
Absorption at 1053 nm (cm <sup>-1</sup> )	1.1x10 <sup>-3</sup> ( $\pm$ 9%)	0.7x10 <sup>-3</sup> ( $\pm$ 24%)	$\leq$ 1.9x10 <sup>-3</sup>
Absorption at 3333 nm (cm <sup>-1</sup> )	1.49 ( $\pm$ 19%)	1.46 ( $\pm$ 29%)	$\leq$ 2.0
Refractive index at 1053 nm	1.497 ( $\pm$ 0.01%)	1.522 ( $\pm$ 0.02%)	1.499 $\pm$ 0.003 (LG-770) 1.520 $\pm$ 0.003 (LHG-8)
Finished Thickness (mm)	40.88 ( $\pm$ 1%)	40.91( $\pm$ 1%)	40 (+1-0)
Transmitted wavefront (PV) (waves at 633 nm) <sup>1</sup>	0.21( $\pm$ 39%)	0.22 ( $\pm$ 38%)	$\leq$ 0.333
Transmitted wavefront (Gradient) (waves at 633 nm/cm) <sup>2</sup>	0.010 (-30%+1%)	0.010 (-52%+1%)	$\leq$ 0.0111
PSD1 <sup>3</sup> (nm)	1.29 ( $\pm$ 16%)	1.42 ( $\pm$ 15%)	1.8

<sup>1</sup>Peak-to-Valley; measured over a spatial scale >33mm; <sup>2</sup>Gradient; measured over a spatial scale >33mm; <sup>3</sup>Power spectral density; measured over a special scale from 2.5 to 33 mm; root-mean-square value

**Table 2:** Tab grading description, TAB distribution and maximum allowable use fluence for amplifier slabs

Tab Grade	Maximum Number of Pt damage sites	Maximum Pt damage size ( $\mu$ m)	% of slabs*	Maximum allowed fluence to minimize growth (J/cm <sup>2</sup> at 3 ns equivalent)
1	5	200	27%	11.1
2	5	350	13%	9.3
3	10	500	17%	6.7
4	20	1000	43%	4.7

\*represents % of slabs that have the specified TAB grade using current statistics on damage tested slabs for LHG-8 and LG-770 combined

### 3. SELECTION OF SLABS FOR NIF BEAM LINE

Each of the 192 NIF beam lines is capable of containing up to 18 amplifier slabs, a maximum of 11 in the Main Amplifier (MA) and 7 in the Power Amplifier (PA). Currently, the four operating beam lines use this 11-7 configuration; however, given the recent excellent measured performance of these four beam lines it is clear that NIF can reach it’s energy and power milestones with an 11-3 configuration. Fig. 4 shows a schematic of the large optics in a single NIF beam line, specifically illustrating the orientation, location, and labeling of the amplifier slabs. A laser shot in NIF will have 2 passes through the PA and 4 passes through the MA. Hence, during a laser shot of the “11-7” beam line configuration, the laser pulse will pass through 58 amplifier slabs. The slabs are oriented at Brewster’s angle within the beam line to minimize fresnel reflection losses and to maximize light absorption from the flashlamps. In addition, adjacent slab locations alternate between two mirror image configurations (that we refer to as “even” and “odd”) as shown in Fig. 4. In order to maximize the slab lifetime and laser performance, each slab (which is unique in its properties) is selected for specific amplifier locations. Some key issues that drive the selection rules are: 1) maximizing the amplifier slab life which is likely limited by growth of Pt pre-damaged sites in the glass; 2) maintaining a reasonable gain balance between beam lines; and 3) minimizing the beam “walk off”. Each of these issues is discuss below.

Based on offline laser testing of Pt sites initiated by the scanning QA process, there is a statistical possibility that these initial damage sites can grow beyond their original post-scan size during subsequent use on the NIF laser. The damage growth probability will increase with the fluence that the slab will see in the beam line. If that site were to grow to sizes approaching 3-4 mm, it is possible for the interference of the scattered light from this site with the main beam to cause an intensity spike downstream possibly initiating damage in other optics. In addition, the scattered light from any damage sites increases the fluence on the low-pass pinhole in the spatial filter (see Fig. 4). Currently on-line cameras are used to image the Pt damage sites in the slabs; hence the larger sites can be detected before they can grow beyond a critical size, and the slab can be replaced.

Using an acceptable slab replacement rate, the maximum fluence that a specific slab grade can be exposed to has been calculated (values are shown in Table 2) using the offline growth data described above. Note that the maximum fluence a particular slab will see increases from the MA1 position to the PA7 position. Hence, slabs with the least number and smallest size Pt damage sites (i.e. Tab 1 slabs) are then preferentially placed in highest fluence locations on the beam line. The exact assignment of a specific slab grade to a specific beam line location depends on the number of amplifiers put in the beam line and its corresponding fluence map. For the four active beam lines in NIF, which utilize an 11-7 configuration, TAB 4 slabs occupy locations MA1-9, TAB 3 slabs occupy MA10-11 plus PA1, TAB 2 slabs occupy PA2-5, and TAB 1 slabs occupy PA6-7.

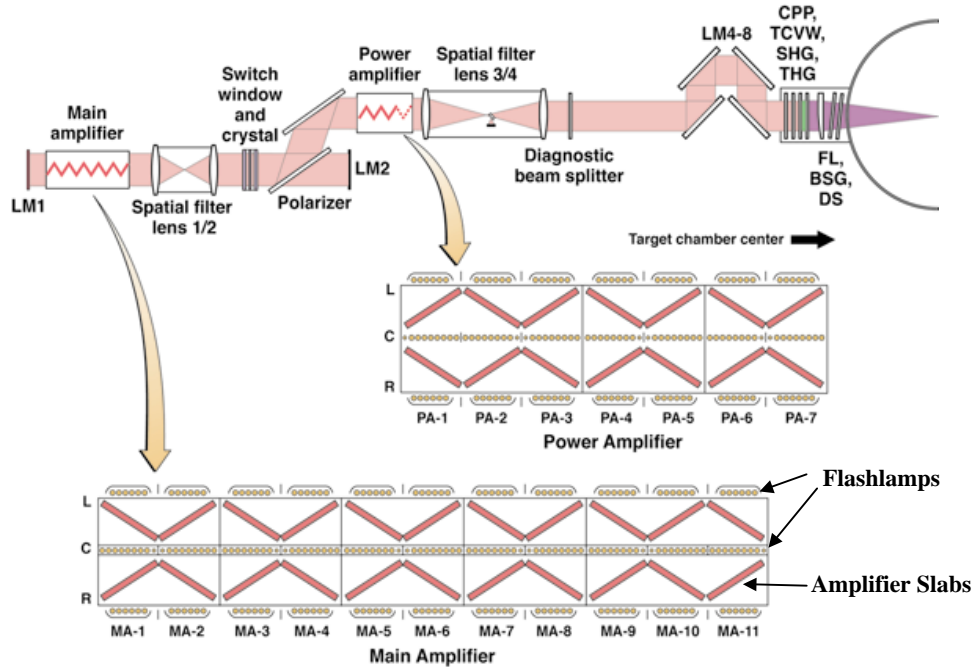


**Fig. 4.** (Top) Schematic illustration of the optics in a single NIF beam line; (Bottom) Location and orientation of amplifier slabs in the MA and PA for two adjacent beam lines.

The second goal of the slab selection process is to ensure gain balance between beam lines. A number of factors can affect the amplifier glass gain (such as absorbing impurities, fluorescence quenching by OH, etc.); however, the quality of the NIF glass is so high and the slab-to-slab statistical variation is so small that these effects are negligible and can be ignored. Another factor that could potentially affect the gain balance is thickness variations between the amplifier slabs. However, the variation in thickness of the finished slabs is small (see Table 1). Therefore, the statistical change in total glass thickness from beam line to beam line is also small and presently can be ignored. Nevertheless, in the future, any laser slabs that need to be refinished (we have allowed sufficient thickness to allow one refinishing) will be 3-4 mm thinner and the effect of thickness variation on the gain balance, will need to be considered. A third factor that can affect the gain balance is the fact we use two different glass compositions that have different emission cross-sections ( $3.9 \times 10^{-20} \text{ cm}^2$  for LG-770 and  $3.6 \times 10^{-20} \text{ cm}^2$  for LHG-8). Therefore variations in the number-per-beam line of each glass type can affect the beam-to-beam gain variation. The general rule to date for maintaining gain balance has been to use the same number of slabs of a particular glass type in each beam line.

The third issue in the slab selection process is the cumulative effects of beam refraction as the light passes through the slabs. Because the slabs are oriented at Brewster's angle to the direction of beam propagation, the beam will be refracted sideways by an amount that depends on the glass thickness and refractive index (see Fig. 5); we refer to this refractive driven movement as a "side-step". Using Snell's Law and basic geometry, it is straightforward to show that the amount of side-step ( $s_i$ ) for a given slab (i) is given by:

$$s_i = \frac{t_i \sin \theta_3}{\cos \theta_2} = \frac{t_i \sin \left( \theta_1 - \arcsin \left( \frac{n_1}{n_{gi}} \sin \theta_1 \right) \right)}{\cos \left( \arcsin \left( \frac{n_1}{n_{gi}} \sin \theta_1 \right) \right)} \quad (1)$$

where  $\theta_1$  is the angle of incidence,  $n_1$  is the environment index, and  $n_{gi}$  and  $t_i$  are the refractive index and thickness of a given amplifier slab, respectively. We also define the term,  $s_n$ , that is the nominal side-step for the "average" slab ( $n_g = 1.05965$ ,  $t = 41.0$  mm). Because the slabs are mounted sequentially in "mirror image" positions (see Fig 4) then the side-step in one direction is offset by a corresponding side-step in the opposite direction as the beam propagates through the beam line. Thus, if all slabs have exactly the same composition (refractive index) and thickness then the cumulative offset is zero after passing through an even number of slabs. However, if there are slab-to-slab variations in thickness and glass type in any given beam line then the magnitude of the side-step,  $s_i$ , will also vary. The sum of the side-step variations can cause the beam to "walk-off" from the average position by an amount  $x_i$ :

$$x_i = s_i - s_n. \quad (2)$$

For a specific amplifier (i.e. MA or PA), the total walkoff ( $x_T$ ) is then:

$$x_T = \sum_{\text{even slabs}} x_i - \sum_{\text{odd slabs}} x_i. \quad (3)$$

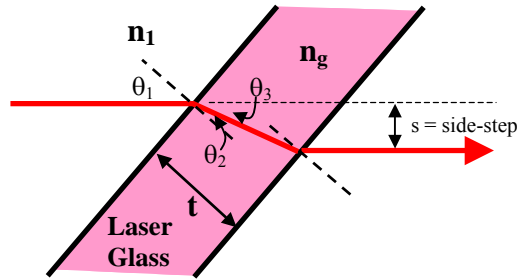


**Fig.5.** Schematic illustration of beam side-step created by laser light refracting through a Brewster-angle mounted amplifier slab.

In order to ensure the beam does not move outside the specified clear aperture the current guideline is that the cumulative walk off ( $x_T$ ) should not exceed  $\pm 1$  mm in any given amplifier (MA or PA). The nominal thickness variation of finished amplifier slabs to date is small (see Table 1), which leads to fairly small changes in the walkoff. Instead, the index difference between two glass types is the driving factor for the walkoff. To minimize walkoff, slabs of the same glass type (LG-770 or LHG-8) are paired together (odd and even) such that the majority of the walkoff is cancelled out. This approach of pairing similar glass types has been effective to date.

#### 4. RECENT TECHNICAL CHALLENGES

The technical advances needed to make continuous melting successful were a result of a six-year, joint R&D effort between LLNL, Schott, and Hoya. These specific technological developments and associated technical references are listed and briefly described below:

- 1) **Pt-inclusion removal:** Microscopic Pt particles ( $\leq 10\mu\text{m}$ ) in the laser glass can absorb laser light and cause fracture in the glass (laser induced damage). Research on their formation and dissolution has led to a redox-controlled process for minimizing the number and size of inclusions in the glass [4,5,10,11].
- 2) **OH removal:** Hydroxyl (OH) groups in the glass quench the fluorescence of the Nd and reduce the laser output energy. Our research on the chemical mechanism of OH removal (dehydroxylation) using reactive gas bubbling and the incorporation of this information in numerical process models has led to a  $10\times$  reduction of OH content of continuously melted glass [4,12,13].

- 3) **Fracture prevention:** Phosphate laser glasses are prone to fracture due to their low fracture toughness and high thermal expansion. Finite element heat transport and stress analysis combined with the identification of various stress sources and research in crack growth have led to improvements in the annealing process that eliminate fracturing [14-16].
- 4) **Impurity minimization:** Metal ion impurities (such as Fe and Cu)  $\geq 10$  parts-per-million level can increase the optical absorption of the glass above acceptable limits and also quench the Nd fluorescence. New analytical techniques to quantify impurity levels combined with research on the absorption and quenching characteristics of these impurities has led to improved specifications and QA procedures for both the laser glass and the raw materials [8,17].
- 5) **Homogeneity:** Laser glass requires a refractive index uniformity (i.e. optical homogeneity) of about one-part-per-million involving advanced forming technologies. The details of this technology are proprietary.
- 6) **Quality assurance:** A number of unique quality-assurance tools have been developed to inspect large optical glass plates at a high rate. These tools include large-aperture (24-inch) phase-measuring interferometers and large-aperture raster-scanning laser damage testers to detect Pt inclusions.

In the past two years, a new set of technical developments has focused on the finishing, long-term stability, and use of the amplifier slabs in the NIF laser system. Three of the challenges (hazing, weathering, and mounting fracture) and their mitigations are discussed in the following sub-sections.

#### 4.1 Hazing

The large optics on NIF require high quality optical surfaces ( $\lambda/3$  surface finish and 2-10 Å root-mean square (rms) surface roughness) in order to maintain a uniform wavefront and to minimize surface scatter of the passing laser light [18,19]. Increased scatter due to increased roughness degrades the beam quality by producing unacceptable intensity modulation (noise) that both increases the probability for damage to downstream optics and increases the fluence on the spatial filter pinholes.

Most of NIF optics in the 1053nm section of the laser, including the laser slabs, are finished using a cerium oxide slurry. After final polishing, the optic must be cleaned to remove the slurry, and it is well known that residual slurry must not be allowed to dry on the glass surface otherwise the surface will be stained. According to Karow [19], “the very large number of these tiny particles is the source of haze, stains, and spots on the surface”. The discussion below describes a proposed chemical mechanism by which the surface roughness of phosphate laser glass can increase by failure to remove residual slurry.

The chemical reactivity of residual slurry with a phosphate glass surface is very high compared to that for fused silica or BK-7. A series of laser phosphate glass test samples [20] were pitch polished using 0.5  $\mu\text{m}$  ceria particles and then washed by different methods that left varying amounts of residual slurry to on the dry surface [20]. Note in all cases any traces of the residual slurry could be not seen with the un-aided eye. Upon re-washing the samples with water, the glass surfaces appeared hazy, which scaled with the amount of residual slurry that remained on the surface. Fig. 6 shows a highly hazed versus haze-free laser glass surface when viewed in a dark room using a high intensity fiber light. The surface topology of the glass surface, as measured by white light optical profilometry and atomic force microscopy, showed that the haze appearance is a result of scatter from shallow surface pits (150 nm - 20  $\mu\text{m}$  wide x  $\sim 15$  nm deep) (see Fig. 7). The rms roughness for the hazed glass is 1.04 nm versus 0.20 nm for the haze-free glass.

We propose that the surface pits result from reaction of the glass with condensed liquid at the slurry particle-glass interface that produces water-soluble phosphate products that dissolves away with subsequent water contact. We also suggest that the dissolved glass products that normally remain in the slurry affect the solution pH and greatly enhance pit formation. This view is supported by polishing experiments on phosphate glass using new (never used) slurry that did not cause pits, while a previously used slurry and new slurry containing dissolved KOH (pH=10) did cause pits [20]. Also, chemical analysis of the rinse solution after re-washing the slabs showed that removed material contained dissolved glass components [20]. The polishing of oxide glass is known to occur by a combination of chemical and mechanical processes because material removal occurs by both chemical interactions (particularly between  $\text{CeO}_2$  and glass in the presence of water) and by mechanical interactions (such as indentation fracture of the glass surface by an abrasive particle) [21-23]. Hence the chemical reactivity of a stagnant  $\text{CeO}_2$  polishing particle with the glass surface is not surprising. A schematic summarizing the proposed sequence and mechanism for pit formation is illustrated in Fig. 8.

Working with our vendor, we have developed a glass-cleaning procedure to remove any residual slurry from the optic at the end of the polishing step. Immediately after removing the optic from the polishing lap it is rinsed with copious amount of de-ionized water followed by a mechanical surface wipe using a soft cloth. This washing method has been

proven effective in minimizing the haze (i.e. reducing micro-roughness) of the surface of the finished amplifier slabs and is now part of our production process. Figures 6 and 7 illustrate how this rigorous cleaning cycle greatly improves the surface quality; the left side in each figure represents samples that have not been cleaned with the new process and the right side represents samples subjected to the new cleaning procedure [20].

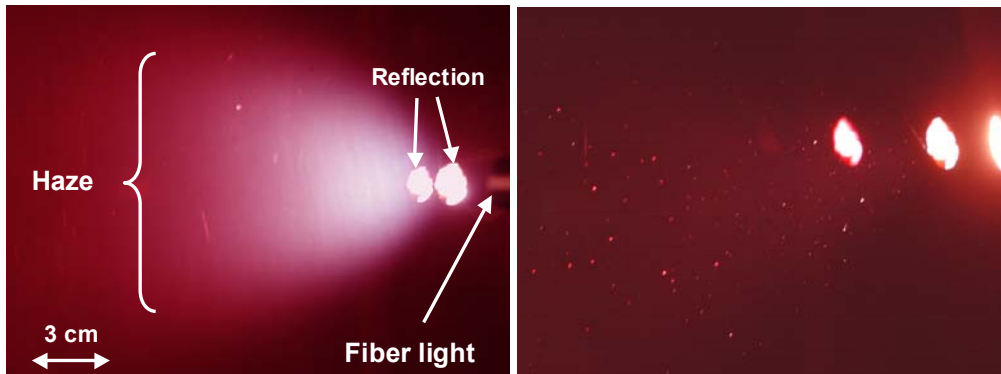


**Fig. 6:** Photographs of the surface scatter observed from a highly hazy laser glass sample (left) and an essentially haze-free sample (right). Images were taken in a dark room upon viewing the diffuse reflectance from a high intensity fiber light. The particles observed in the image on the right were intentionally left on surface in order to distinguish (i.e. focus on) the surface [20].

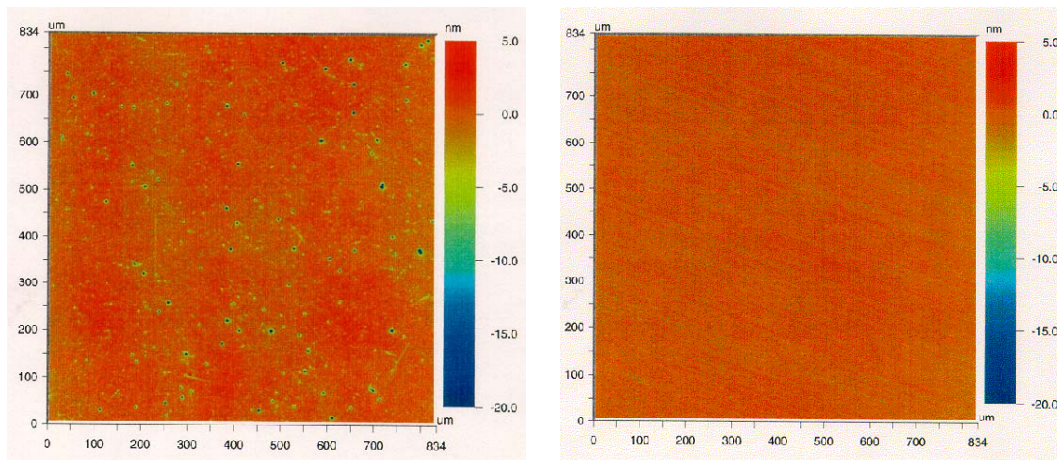


**Fig. 7.** Surface contour measured by a white-light optical profilometer over a  $834 \times 834 \mu\text{m}^2$  aperture for a laser glass with a hazed surface (left) and with a haze-free surface (right) [20]. The colored vertical bar with each image denotes the depth scale in nm.

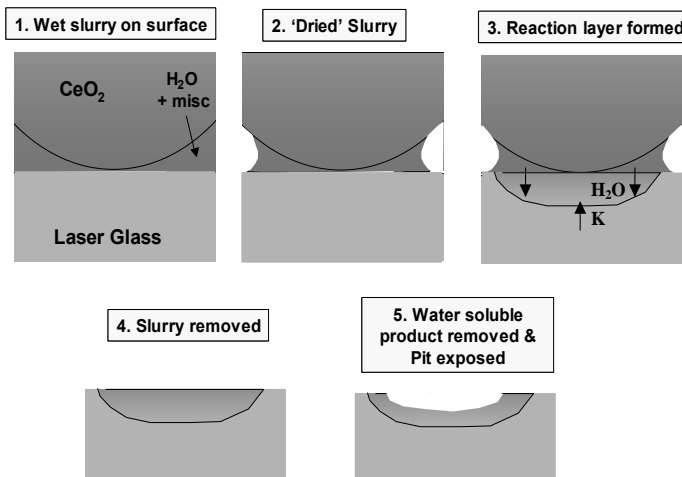


**Fig. 8:** Schematic illustration of pit formation in phosphate glass when a residual  $\text{CeO}_2$  slurry particle ‘dries’ on surface [20].

## 4.2 Weathering

Small transmission losses in the laser slabs can significantly degrade the laser output energy. In particular, transmission losses due to degradation of the precision polished optical surface by glass weathering can be a significant performance issue. For example, as little as a 0.1% transmission loss per slab due to degradation of the slab's surfaces (0.05% per surface) would give more than 5% loss in output energy.

Glass weathering is due to reaction of the glass surface with either water vapor or other gases (e.g.  $\text{CO}_2$ ). The weathering reactions also typically follow an Arrhenius (exponential) temperature dependence becoming much faster at elevated temperatures. To address this potential concern NIF maintains the amplifier temperature near  $20^\circ\text{C}$  and uses a high purity, “dry” (relative humidity (RH) < 0.1%) purge gas to prevent weathering. Also, during amplifier assembly, we specify minimum exposure times (<30 days) to the ambient humidity conditions of the assembly facility to minimize weathering. In addition, slabs not installed on NIF are stored in hermetically sealed bags with molecular sieve desiccant to ensure the glass is exposed to no more than 0.6% RH upon initial packaging and no more than 5% RH after 30 years of storage (the expected operational lifetime of NIF) (Fig. 9).

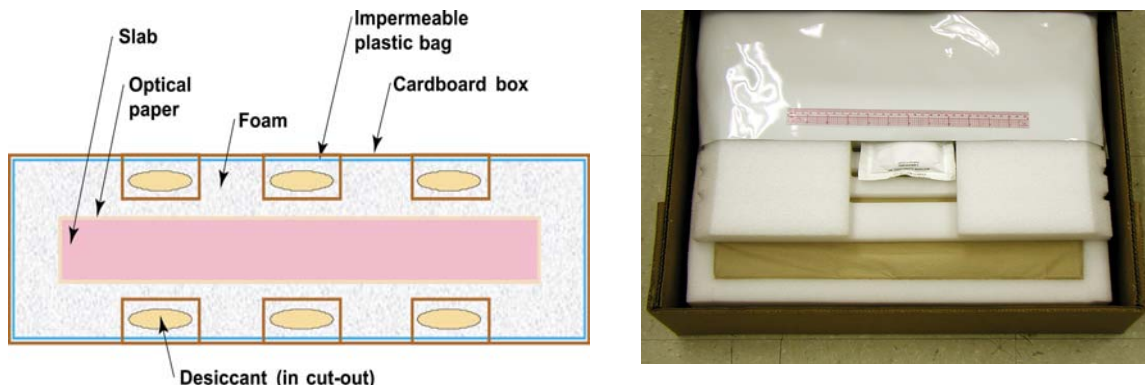


**Fig. 9.** (Left) Schematic showing the packaging scheme of the laser glass slab; (Right) photo showing components of a packaged slab.

The time-temperature-humidity exposure limits for the NIF laser slabs are being quantified by on going measurements on the two laser glasses. To date measurements for LG-770 are largely complete, however much of the work on LHG-8 is still in progress. We are measuring the weathering rate of the glasses by a series of long-time exposure tests at fixed temperature and humidity. Some of the tests run for almost two years (700 days). Because of the extremely slow weathering of these glasses under the NIF amplifier use conditions, we have measured the weathering rate under accelerated conditions, specifically at elevated temperatures and humidity. We are using these data to develop a chemical kinetic model that allows us to extrapolate to the low humidity in use on the NIF. A preliminary model for LG-770 is complete and forms the basis for much of the remaining discussion.

At elevated temperatures, LG-770 weathers faster than LHG-8; for example, at  $50^\circ\text{C}$  the rate is about 10x faster. It was known at the time of development of the LG-770 composition that it would weather at a greater rate than LHG-8 under certain exposure conditions. This is because LG-770 was purposely formulated with as low alumina content as possible to increase the emission cross-section.  $\text{Al}_2\text{O}_3$  is known to increase the durability of phosphate laser glasses. Despite the lower alumina content, our tests show that weathering will not be a problem for LG-770 in the “dry” NIF amplifiers, even over the expected 30-year life.

Based on the data we have for LG-770, the weathering process appears to occur in two phases: (1) an induction period during which no noticeable change in the glass surface quality is observed followed by (2) the onset of measurable production of weathering surface reaction products (Fig. 10). During the induction period we cannot detect any weathering products even with our most sensitive chemical methods. Therefore we feel the induction period is a “grace period” for which there is no measurable degradation in the optical quality of the precision polished glass surface. The induction period is a function of the temperature and relative humidity; under ambient conditions ( $20^\circ\text{C}$  and 50%RH) the induction period is about 200 days for LG-770. The activation energy for the induction period is about 85 kJ/mole and depends on the relative humidity as approximately  $\text{RH}^{3/2}$ . Early data suggests that the induction period for LHG-8 is longer than that for LG-770; this is expected because of the higher  $\text{Al}_2\text{O}_3$  in the LHG-8.

Following the induction period there is a noticeable build-up of products on the surface of the glass. Analysis of the weathering products show that they are primarily KPO compounds (potassium dihydrogen phosphate,  $\text{KH}_2\text{PO}_4$ , is a commonly observed product). The weathering products can be readily dissolved from the glass surface and trace chemical analyses are used to quantify the quantities produced per unit area of glass exposed. These data have been fit to a kinetic model that gives an activation energy for LG-770 of about 120 kJ/mole; the weathering rate was also found to depend on the square of the relative humidity ( $\text{RH}^2$ ). The activation energy for LHG-8 is unknown at this time as we are still in the process of quantifying it.

Our experiments have also shown that under the same exposure conditions (temperature and relative humidity), the quality of the glass finish can dramatically affect the induction period and the rate of weathering. Glass surfaces with an inspection polish or a ground surface degrade much faster than do glasses with a good optical finish. This agrees with our supposition that the weathering occurs near regions of enhanced reactivity such as surface defects left from polishing. For example, the weathering shown in Fig. 10 begins at points on the surface suggesting initiation at a defect; over time more and more of these points appear and eventually form “colonies”. The other observation that supports a defect-initiation model is that unpolished, melted glass surfaces have outstanding durability.

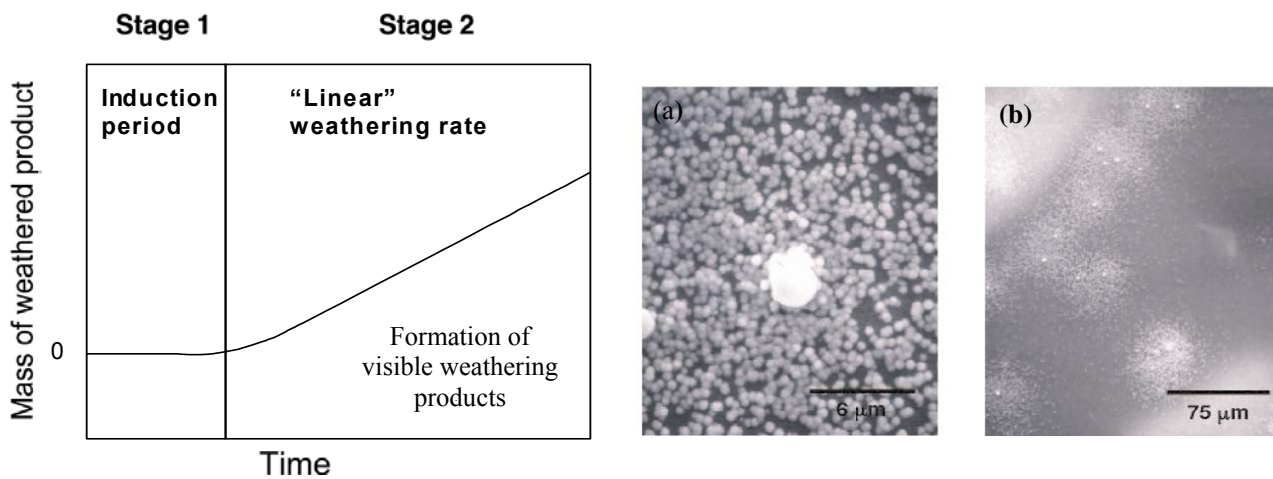


**Fig. 10.** (Left) Schematic representation of the two stages of weathering observed for phosphate laser glasses; (Right) SEM photos of glass weathering products observed after exposure of LG-770 to accelerated weathering conditions (50°C, 100% RH): (a) Growth initiation occurred at the white “dot” shown near the center of the image; clusters of smaller, similarly-shaped weathering sites later grew around this central site giving the impression of a “colony”; (b) The image shows a number of colonies that have developed across the glass surface each characterized by a central white “dot” representing the initiation site. At later times the numerous colonies will coalesce to completely cover the exposed glass surface.

### 4.3 Mounting Fracture

Before installation in NIF, the amplifier slabs are cleaned and then installed in Line Replaceable Units (LRUs) as shown in Fig. 2. Each slab is supported on two ‘soft’ Al alloy buttons (1 cm in diameter) on a stiff metal shelf below the slab. This support is specifically designed to minimize mounting-induced optical distortion. However, despite offline mechanical testing of the button showing that it would not damage the glass, surface fractures were observed on a number of test amplifier slabs at the contact zone between the Al button and the glass. Figure 11 shows a photograph of one of the observed fractures. The fractures were ~1 mm deep and have a semicircle shape (when viewed normal the bottom-edge of the glass) outlining the Al-to-glass contact zone.

The occurrence of these fractures was surprising given the early load test results showed that the buttons would not cause damage. The Al buttons were specifically made from Al 6061 T0 (which has a hardness much lower than laser glass), and designed with a large radius of curvature (25 cm). The combination of the hardness and curvature significantly increase the load required to initiate fracture [24]. In fact, mechanical testing of the Al buttons on laser glass coupons under normal-load conditions showed no glass damage even at loads up to  $4 \cdot 10^4$  N (9000 lbf). However, in use tests of the assembled LRUs, the buttons were observed to cause fractures in the slabs at loads of approximately half the weight of an amplifier slab (~270 N or ~60 lbf).

The observed fractures have many similarities to those produced by indentation with a hard blunt object (so-called Hertzian fracture [24,25]). When a spherical indenter of radius  $r$  is normally loaded onto a brittle substrate, fracture will form in the shape of a cone (“Hertzian” cone) originating at the circumference of the elastic contact zone between the sphere and glass. Ideal Hertzian fracture assumes: 1) the hardness of the indenter is greater than the substrate; 2) the load is applied only normal to the substrate; and 3) only brittle fracture is occurring. Based on this, the load to initiate fracture is given by:

$$P_c = A r, \quad (4)$$

and the load to propagate fracture is given by:

$$P = \frac{K_{Ic}}{\chi} c^{3/2}, \quad (5)$$

where  $A$  is Auerbach’s constant that is material dependent (N/m),  $r$  is the radius of curvature of the indenter (m),  $K_{Ic}$  is the fracture toughness of the substrate (MPa/m<sup>1/2</sup>),  $c$  is the length of the cone crack (m), and  $\chi$  is the another material constant. Note Eq. 5 is valid only when  $P > P_c$ .  $A$  has been previously measured for laser glass as  $1.7 \cdot 10^4$  N/m (3.8 lbf/mm), which gives a critical load at failure ( $P_c$ ) of about 4500 N (1000 lbf). This is well above the load at which fracture was observed on edge of the amplifier slabs. Using  $\chi=0.05$  (typical for glass), and  $P=270$  N (60 lbf) in Eq. 5, we get a crack length of  $\sim 1$  mm, which is the similar to the observed crack length. Hence, some effect caused the initiation load to drop significantly; we believe this is caused by deviation in the button loading from the ideal Hertzian case

The Al button contact with laser glass deviates from ideal Hertzian loading for two reasons. First, the Al button has a lower hardness than the laser glass. Second, the entire load is not normal to the glass substrate as was assumed in the design and load testing, rather there exists a significant frictional or a tangential load component. Two observations indicate the presence of a tangential load. First, the observed fractures are asymmetric with respect to the cone shape fracture in contrast to that expected for ideal normal (Hertzian) loading conditions; this suggests that the net load is not normal to the substrate [24]. Second, there was aluminum deposit on the glass surface at the Al-to-glass contact zone (see Fig. 11), suggesting tangential loads and sliding caused the aluminum to rub off the button. Note no aluminum deposit was observed on the test coupons because the Instron® sample mounts are design to ensure the load is applied normal to the surface.

Figure 11 also shows a comparison of the calculated stress distribution during Hertzian loading with and without a tangential load [24]. With a tangential load, the tensile stress at the leading edge is reduced, while the tensile stress at the trailing edge is increased. Hence the initiation load for fracture ( $P_c$ ) at the trailing edge would decrease with increase in tangential load. The amount of drop in the initiation load can be quite high. Experiments on the effect of different metals sliding across the glass surfaces was examined more than 60 years ago by Ghering et. al. [26]. For iron,  $P_c$  dropped from 35 kgf (without a tangential load) to 0.23 kgf (with a tangential load); this is  $>100x$  decrease in the initiation load. Chiang et. al. [27] have performed calculations showing the effect of tangential forces on the initiation load; their results show that  $P_c$  could drop by orders of magnitude with the addition of a tangential load.

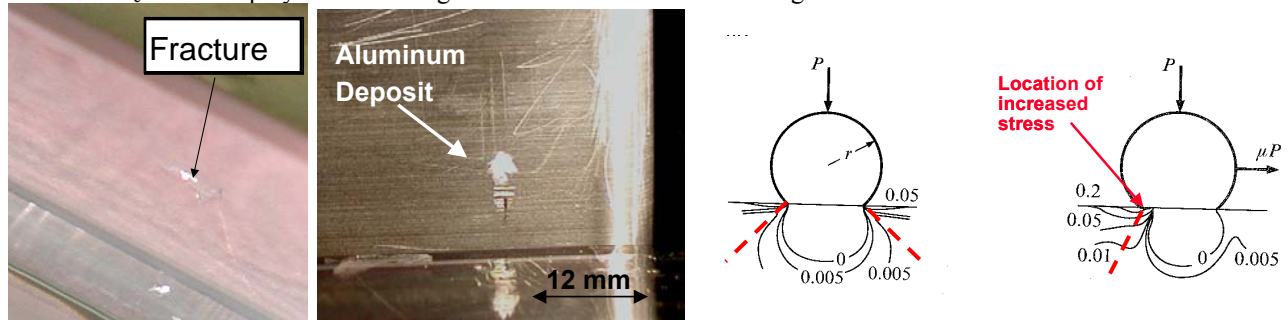


**Fig. 11.** (Left) Off-axis view of the cladding edge of amplifier slab illustrating the fracture observed at the contact between the aluminum button and glass surface; (Middle) Al deposit found on amplifier slab edge where fracture was observed; (Right) Comparison of normalized stress contours (solid lines) and expected crack propagation (dashed lines) upon ideal Hertzian loading and modified Hertzian loading with a tangential load. Stress distribution after Lawn [24].

In order to minimize tangential force effects, a hard/thin stainless steel shim is now placed between the button and the glass surface. With this modification, concentrated frictional forces and sliding occur at the button-shim interface, not the glass-shim interface. To date, this mitigation step has been effective in preventing surface fractures to the laser slabs.

## ACKNOWLEDGEMENTS

The authors would like to thank all the members of the laser glass production team including co-workers at LLNL, Schott Glass Technologies, Hoya Corporation USA, and Zygo Corporation. The authors would also like to thank the members of the Amplifier LRU Working Group for their contributions on the mounting fracture mitigation and the Optics Processing Laboratory (OPL) crew at LLNL for their contributions on the hazing mitigation. This work was performed under the auspices of the U.S. Department of Energy by the University of California, Lawrence Livermore National Laboratory under contract No. 7405-ENG-48.

## REFERENCES

1. J. Murray, "Overview of the National Ignition Facility", *SPIE* **3492 Supplement** (1998) 1.
2. E. I. Moses, J. H. Campbell, C. Stolz, C. Wuest, "The National Ignition Facility: The World's Largest Optics and Laser System", *SPIE* **5001** (2003) 1.
3. M. Andre, M. Novaro, D. Schirmann, *Chocs. Rev. Sci. Techn. Direct. Appli. Milit.* **13** (1995) 73.
4. J. H. Campbell, T. I. Suratwala, "Nd-doped phosphate glasses for high-energy/high peak power lasers", *J. of Non-Cryst. Solids*, **263&264** (2000) 318.
5. J. H. Campbell, T. I. Suratwala, C. B. Thorsness, J. S. Hayden, A. J. Thorne, J. M. Cimino, A. J. Marker III, K. Takeuchi, M. Smolley, G. F. Ficini-Dorn, "Continuous melting of phosphate laser glasses", *J. of Non-Cryst. Solids*, **263&264** (2000) 342.
6. J. H. Campbell, "Recent advances in Phosphate Laser Glasses for High Power Applications", LLNL Report, UCRL-JC-124244 (1996).
7. T. Suratwala, C. Thorsness, J. Campbell, S. Krenitsky, J. Cimino, A. Thorne, J. Hayden, K. Takeuchi, K. Suzuki, K. Yamamoto, "Technical advances in the continuous melting of phosphate laser glass," in *Inertial Fusion Sciences and Applications*, ed. K. Tanaka, D. Meyerhofer, J. Meyert-ter-Vehn, Elsevier (2002) 540-543.
8. P. R. Ehrmann and J. H. Campbell, "Nonradiative energy losses and radiation trapping in neodymium-doped phosphate laser glasses", *J. Am. Ceram. Soc.* **85** (2002) 1061.
9. R. Boland, "Computer Control and Process Monitoring of Electrolytic In-Process Dressing of Metal Bond Fine Diamond Wheels for NIF Optic", *SPIE* **3782** (1999) 61.
10. J. H. Campbell, E. P. Wallerstein, H. Toratani, E. Meissner, "Effects of process gas environment on platinum inclusion density and dissolution rate in phosphate laser glasses", *Glastech. Ber. Glass Sci. Technol.* **68** (2) (1995) 59-69.
11. J. H. Campbell, E. P. Wallerstein, J. S. Hayden, D. L. Sapak, D. E. Warrington, A. J. Marker, "Effects of melting conditions on platinum inclusion content in phosphate laser glasses", *Glastech. Ber. Glass Sci. Technol.* **68** (1) (1995) 11-21.
12. C. B. Thorsness, T. I. Suratwala, R. A. Steele, J. H. Campbell, J. S. Hayden, S. A. Pucilowski, K. Suzuki, "Dehydroxylation of Phosphate Laser Glass", *SPIE* **4102** (2000) 175-194.
13. P. R. Ehrmann, K. Carlson, J. H. Campbell, C. A. Click, and R. K. Brown, "Neodymium fluorescence quenching by hydroxyl groups in phosphate laser glasses", submitted *J. of Non-Cryst. Solids* (2003).
14. T. I. Suratwala, R. A. Steele, G. D. Wilke, J. H. Campbell, "Effects of OH content, water vapor pressure, and temperature on sub-critical crack growth in phosphate glass", *J. of Non-Cryst. Solids* **263&264** (2000) 213-227.
15. S. Crichton, M. Tomozawa, J. Hayden, T. Suratwala, J. Campbell, "Sub-Critical Crack Growth in a Phosphate Laser Glass," *J. Am. Cer. Soc.* **82**(11) (1999) 3097-104.
16. J. S. Hayden, A. J. Marker III, T. I. Suratwala, J. H. Campbell, "Surface tensile layer generation during thermal annealing of phosphate glass," *J. of Non-Cryst. Solids* **263&264** (2000) 228.
17. P. R. Ehrmann, J. H. Campbell, T. I. Suratwala, J. S. Hayden, D. Krashkevich, K. Takeuchi, "Optical loss and Nd<sup>3+</sup> non-radiative relaxation by Cu, Fe, and several rare earth impurities in phosphate laser glasses", *J. of Non-Cryst. Solids* **263&264** (2000) 251-262.
18. C. Stolz, J. Menapace, M. Borden, A. Slomba, C. Kiikka, S. Gelman, "Status of Optical Finishing for the National Ignition Facility", in *Optical Fabrication and Testing*, OSA Technical Digest (2002) 67.
19. H. Karow, *Fabrication Methods for Precision Optics*, John Wiley & Sons, Inc., New York (1993).
20. T. Suratwala, P. Miller, P. Ehrmann, R. Steele, "Polishing slurry induced surface haze on phosphate laser glasses", submitted to *J. of Non-Cryst. Solids* (2003).
21. L. Cook, "Chemical Processes in Glass Polishing", *J. Non-Cryst. Solids* **120** (1990) 152.
22. T. Izumitani, in: *Treatise on Material Science and Technology*, Vol 17, eds. M. Tomozawa and R. Doremus, Academic Press, New York (1979) 115.
23. M. Tomozawa, K. Yang, H. Li, S. Murarka, "Basic Science in Silica Glass Polishing", *Mat. Res. Soc. Symp. Proc.* **337** (1994) 89.
24. B. Lawn, "Fracture of Brittle Solids- 2<sup>nd</sup> Edition", Cambridge University Press, Cambridge, UK (1993).
25. H. Hertz, *Hertz's Miscellaneous Papers*, Chapters 5 & 6, Macmillan, London, UK (1896).
26. L. Ghering and J. Turnbull, "Scratching of Glass by Metals", *Bull. Am. Ceram. Soc.* **19**(8) (1940) 290.
27. S. Chiang and A. Evans, "Influence of Tangential Force on the Fracture of two contacting elastic bodies", *J. Am. Ceram. Soc.* **66**(1) (1983) 4.